Pergamon

0038-1101(95)00115-8

Solid-State Electronics Vol. 39, No. 2, pp. 217–223, 1996

0038-1101/96 $15.00 + 0.00

DUAL-CARRIER TRANSPORT MODEL OF SPRITE DETECTORS

FRANK J. EFFENBERGER and GLENN D. BOREMAN

Center for Research and Education in Optics and Lasers, Department of Electrical and Computer Engineering, University of Central Florida, Orlando, FL 32816, U.S.A.

(Received 12 April 1995)

Abstract—A numerical model for signal-processing-in-the-element (SPRITE) detectors is developed that incorporates both hole and electron motion, the effects of space charge and varying field, and boundary conditions. The model is used to generate a spatial-frequency response for a rectangular SPRITE structure. Further, we use this model to investigate two improved SPRITE structures: the tapered detector and the modulation-doped detector.

NOTATION

Notes: Replace x with n or p to obtain symbol pertaining to electrons or holes, respectively. Subscript i refers to finite variable segment or boundary number. All primed variables are normalized.

z	distance (m)
L	length of detector (m)
A_i	boundary area (m^2)
V_i	segment volume (m^3)
t	time (s)
p_i	hole density (m^{-3})
n_i	electron density (m^{-3})
P_i	donor density (m^{-3})
N_i	acceptor density (m^{-3})
J_x	current density (Am^{-2})
I_i^x	current (A)
E	electric field (Vm^{-1})
q	charge of electron (C)
ϵ	dielectric constant (Fm^{-1})
Φ_i	electric flux (Vm)
D_x	diffusivity ($m^2 s^{-1}$)
μ_x	mobility ($m^2 V^{-1} s^{-1}$)
G	generation rate ($m^{-3} s^{-1}$)
τ_b	bimolecular lifetime ($m^{-3} s$)
τ_m	minority lifetime (s)
R_Q	charge ratio
Q_b	bias charge (C)
Q_d	dopant charge (C)
R_G	generation ratio (C)
P_b	background charge (C)
R_μ	mobility ratio
R_N	noise voltage ratio
U_N	noise voltage (V)
U_0	nominal bias voltage (V)
R_Φ	electric flux ratio
Φ_d	dopant induced flux (Vm)
Φ_0	nominal bias flux (Vm)
$v_{nominal}$	nominal scan speed (ms^{-1})
$\bar{\alpha}$	average normalized drift speed (ms^{-1})
v_c	surface recombination velocity (ms^{-1})
R_c	surface velocity ratio
I_c	surface current (A)

1. INTRODUCTION

The signal-processing-in-the-element (SPRITE) detector is widely used in infra-red imaging applications. These detectors work by utilizing the drift motion of the photogenerated carriers to transfer and delay the detected signal in space and time, respectively. This concept has been applied to create monolithic time-delay-and-integration (TDI) detectors, eliminating most of the circuitry normally required for the implementation of such a system.

The basis for the operation of SPRITE detectors is the constant drift velocity of the minority carriers. The drift velocity depends on the effective mobility of these carriers and the electric field impressed on the semiconductor. While linear analytic models[1, 2] can be derived when both of these quantities are assumed constant, they in fact vary over the extent of the detector. This variation of drift velocity results in the degradation of the modulation transfer function (MTF) of the detector.

This effect was first analyzed using an ambipolar approximation to reduce the consideration to only the minority carriers[3]. Through consideration of the effect of excess carriers on the mobility and the electric field, the width of the detector was varied in the along-scan direction such that the change in cross-sectional area exactly compensated for the change in both field and mobility. Detectors were fabricated with their widths tapered according to this analysis, and measurement of their MTF showed improvement over the non-tapered devices[4]. While this approach seems adequate from a design perspective, it does not allow a complete theoretical prediction of the effect of background-induced variations. More recent analyses have included the variation of generation effect and have used numerical integration

to study the behavior of devices of arbitrary length and taper[5,6]. This more complete model was used to compute the responsivity and revealed an intrinsic saturation in output signal in SPRITE detectors[7].

In this paper, the analysis presented shall improve on the previous work in several ways. First, and most fundamentally, the ambipolar approximation will not be used. While this is unprecedented in SPRITE literature, this dual carrier electrostatic semiconductor model will be more flexible and accurate than previous models, and will allow the investigation of new structure designs. Second, the signal response will be computed using a scanned impulse input. The resulting output will be Fourier analyzed to produce the MTF response of the detector. This is more in keeping with the device's imaging function. In Section 2, the theoretical basis of the model used in this paper will be described. Section 3 will explain the details of the numerical implementation used. The results for rectangular and tapered SPRITEs will be given in Section 4. A new type of structure, the modulation-doped SPRITE, will be introduced in Section 5. Finally, Section 6 will contain the conclusions we can draw from this work.

2. THEORETICAL BASIS

All the previous literature has utilized the ambipolar approximation in the analysis of SPRITE detectors. As the lifetime and background doping level of HgCdTe are improved, the ambipolar description becomes less adequate. The approach taken in this paper will be to use a dual-carrier electrostatic model of electrical behavior in the SPRITE semiconductor. The hole and electron densities, denoted p and n, respectively, are determined by two interrelated continuity equations:

$$\frac{dp}{dt} = -\frac{\nabla \cdot \mathbf{J}_p}{q} - \frac{pn}{\tau_b} + G,$$
$$\frac{dn}{dt} = \frac{\nabla \cdot \mathbf{J}_n}{q} - \frac{pn}{\tau_b} + G. \tag{1}$$

The current densities are driven by diffusion and drift:

$$\mathbf{J}_p = -qD_p\nabla p + q\mathbf{E}\mu_p,$$
$$\mathbf{J}_n = qD_n\nabla n + q\mathbf{E}\mu_n. \tag{2}$$

Finally, Gauss's law:

$$\epsilon\nabla \cdot \mathbf{E} = q[P + p - N - n], \tag{3}$$

is considered, where ϵ is the permeability, and P and N are the positive (donor) and negative (acceptor) dopant concentrations. It should be noted here that the lifetime used in eqns (1), τ_b, is the bimolecular (two-body) recombination time, which is related to the minority lifetime, τ_m, by the relation $\tau_b = P\tau_m$.

SPRITE structures typically have high length-to-width and length-to-thickness ratios, and can be conveniently described with one-dimensional models. In terms of numerical complexity, such models are simpler and faster. However, the effect of device shape and taper are important to this analysis, and these features are markedly two- or even three-dimensional. If it is assumed that the SPRITE is a rectangular solid with only a slowly varying width, then a modified one-dimensional set of equations can be written to describe the device.

To do this, it is convenient to write the equations in the form where the current density and electric field are integrated over the transverse directions. We let the z axis be parallel to the long axis of the SPRITE. Assuming that the current densities and electric field are constant over any individual cross-sectional area of the device, $A(z)$, then:

$$I^p(z) = J_p(z)A(z), \quad I^n(z) = J_n(z)A(z),$$
$$\Phi(z) = E(z)A(z), \tag{4}$$

where I_p, I_n are the hole and electron currents, and Φ is the electric flux. Equations (1)–(4) are the basis for the model.

3. NUMERICAL METHOD

Given the above set of equations, the differentials must be discretized so that they can be evaluated. We define normalized variables to preserve the accuracy of the numerical computation. This normalization also aids in the interpretation of the input parameters and the output results of the model.

The discretization of the equations can most easily be viewed by considering the detector to be divided into m segments, as pictured in Fig. 1 where $m = 12$ for illustrative purposes ($m = 100$ was actually used). Each segment has an equal thickness, Δz, along z. We number these elements from 1 to m. These elements are bounded by planes, numbered 0 to m, each perpendicular to the z axis. Each element is characterized by a volume, V_i, and the densities of the holes, electrons, donors, and acceptors are denoted p_i, n_i, P_i, and N_i, respectively. The boundary planes are described by an area, A_i, the hole current, I_i^p, the electron current, I_i^n, and the electric flux Φ_i.

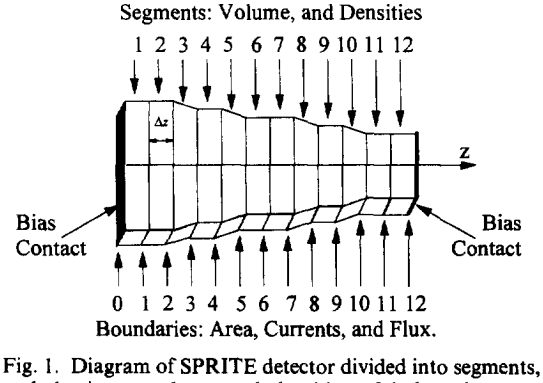

Fig. 1. Diagram of SPRITE detector divided into segments, each having a volume and densities of holes, electrons, acceptors and donors. The boundaries between the segments have an area, hole and electron currents, and flux associated with them.

The basic eqns (1)–(4) can be written in terms of these discrete variables by approximating the z derivatives involved by their finite-difference equivalents. This produces:

$$\frac{\mathrm{d}p_i}{\mathrm{d}t} = \frac{I_{i-1}^p - I_i^p}{qV_i} - \frac{p_i n_i}{\tau_b} + G,$$

$$\frac{dn_i}{\mathrm{d}t} = \frac{I_i^n - I_{i-1}^n}{qV_i} - \frac{p_i n_i}{\tau_b} + G, \tag{5}$$

$$I_i^p = qA_i D_p \frac{p_i - p_{i+1}}{\Delta z} + q\Phi_i \mu_p \frac{p_i + p_{i+1}}{2},$$

$$I_i^n = qA_i D_n \frac{n_{i+1} - n_i}{\Delta z} + q\Phi_i \mu_n \frac{n_i + n_{i+1}}{2}, \tag{6}$$

$$\Phi_i - \Phi_{i-1} = q\frac{V_i}{\epsilon}[P_i + p_i - N_i - n_i]. \tag{7}$$

Normalized variables will be indicated by the prime (′) notation. The independent variables, z and t are most easily normalized to the device length, L, and the minority carrier lifetime, τ_m, thus:

$$z' = \frac{z}{L}, \quad t' = \frac{t}{\tau_m}. \tag{8}$$

Because we are interested in studying the effect of device taper, the area of the boundaries and the volumes of the elements will vary over the length of the device. Here, these variables are normalized to A_0 and V_0:

$$A_i' = \frac{A_i}{A_0}, \quad V_i' = \frac{V_i}{V_0}, \tag{9}$$

where A_0 is the area of the zeroth boundary, and V_0 is defined to be the product $A_0\Delta z$. The carrier and dopant densities are normalized to the concentration of donors in the first segment of the device. This yields:

$$p_i' = \frac{p_i}{P_1}, \quad n_i' = \frac{n_i}{P_1},$$

$$P_i' = \frac{P_i}{P_1}, \quad N_i' = \frac{N_i}{P_1}, \tag{10}$$

The currents are normalized to the bias current applied to the device I_0. The electric flux is normalized to the value of Φ_0 required to establish the bias current. This produces:

$$I_i'^p = \frac{I_i^p}{I_0}, \quad I_i'^n = \frac{I_i^n}{I_0}, \quad \Phi_i' = \frac{\Phi_i}{\Phi_0}. \tag{11}$$

We can write eqns (5)–(7) in a dimensionless form:

$$\frac{\Delta p_i'}{\Delta t'} = R_Q \frac{1}{V_i'} \frac{I_{i-1}'^p - I_i'^p}{\Delta z'} - p_i' n_i' + R_G,$$

$$\frac{\Delta n_i'}{\Delta t'} = R_Q \frac{1}{V_i'} \frac{I_i'^n - I_{i-1}'^n}{\Delta z'} - p_i' n_i' + R_G, \tag{12}$$

$$I_i'^p = R_\mu \left[R_N A_i' \frac{p_i' - p_{i+1}'}{\Delta z'} + \Phi_i' \frac{p_i' + p_{i+1}'}{2} \right],$$

$$I_i'^n = R_N A_i' \frac{n_{i+1}' - n_i'}{\Delta z'} + \Phi_i' \frac{n_i' + n_{i+1}'}{2}, \tag{13}$$

$$\Phi_i' - \Phi_{i-1}' = R_\Phi V_i' [P_i' + p_i' - N_i' - n_i'] \Delta z'. \tag{14}$$

The differential of the normalized distance is now given by:

$$\Delta z' = 1/m. \tag{15}$$

Five dimensionless numbers are introduced that contain all of the parameters of the problem. Each can be thought of as a ratio of two physical properties:

$$R_Q = \frac{I_0 t_m}{qP_0 A_0 L} = \frac{Q_b}{Q_d}, \quad R_G = \frac{Gt_m}{P_0} = \frac{P_b}{P_0},$$

$$R_\mu = \frac{m_p}{m_n}, \quad R_N = \frac{qP_0 m_n A_0 V_N}{I_0 L} = \frac{U_N}{U_0},$$

$$R_\Phi = \frac{qP_0 A_0 L}{F_0 e} = \frac{F_d}{F_0}. \tag{16}$$

The charge ratio, R_Q, is the ratio of the bias charge flowing in one minority lifetime, Q_b, and the total dopant charge in the device, Q_d. The generation ratio, R_G, is the ratio of the equilibrium carrier concentration resulting from generation, P_b, and the dopant concentration, P_0. The mobility ratio, R_μ, is the ratio of the hole and electron mobility. The noise–voltage ratio, R_N, is the ratio of the equivalent-noise voltage, U_N, driving the diffusion process and the normal-bias voltage, U_0. Finally, the electric-flux ratio, R_Φ, is the flux that would result from a positive charge equal to the amount of donor dopant present in the device, Φ_d, over the flux required to establish the bias current.

The scan velocity v, is nominally equal to the speed of the minority carriers:

$$v_{\text{nominal}} = \mu_p E. \tag{17}$$

Because we are using normalized coordinates, we write the following to obtain the normalized nominal scan velocity, v':

$$v'_{\text{nominal}} = \frac{\tau}{L} v_{\text{nominal}} = \frac{\tau \mu_p E}{L} = R_Q R_\mu. \tag{18}$$

To obtain the response of any detectors, eqns (18)–(20) must be integrated in time. The choice of the time increment, $\Delta t'$, is critical for convergence. In this work, the increment used is:

$$\Delta t' = \frac{1}{m^2 R_Q R_\mu \tilde{\alpha}}. \tag{19}$$

Here, m^2 helps to insure that the numerical code will converge, because it is of the same order (m^2) as the second derivative implicit in eqns (12) and (13). The inclusion of the scanning speed further improves stability, and it results in the scanned spot moving $1/m$ elements per time increment. The use of a

Table 1. The values of the six dimensionless ratios used in this work. Of note is the particularly high value of R_Φ. This corresponds to the high strength of the electrostatic interaction

Dimensionless ratio	Typical value
R_Q	1.4
R_G	0.04
R_μ	0.1
R_N	0.005
R_Φ	1500
R_C	0.004

correction factor, $\bar{\alpha}$, is made necessary by the departure of the ambipolar drift velocity from the nominal value. This factor, $\bar{\alpha}$, is the average normalized ambipolar velocity over the detector length.

To incorporate boundary conditions, the assumption is made that the minority carriers exhibit a fixed recombination velocity, v_c, at the ends of the detector. It is also assumed that the detector is biased with a constant current equal to I_0. These two assumptions result in eqns (20) and (21) for the normalized hole and electron currents at the boundaries:

$$I'^p_0 = -R_C p'_1, \quad I'^n_0 = 1 - I'^p_0. \tag{20}$$

$$I'^p_m = R_C A'_m p'_m, \quad I'^n_m = 1 - I'^p_m. \tag{21}$$

The new dimensionless ratio R_C is given by:

$$R_C = \frac{v_c A_0 q P_0}{I_0} = \frac{I_C}{I_0}, \tag{22}$$

where I_C is the surface current resulting from a minority-carrier concentration equal to the majority-dopant concentration. These relations for the terminal currents ensure that an equal amount of positive and negative charge are always present in the detector volume, which produces the required condition of total charge neutrality.

In all preceding models, a rather ad hoc approach was taken in that it was assumed that the readout voltage was proportional to the total charge contained within the readout region. In this model, the normalized output voltage, U'_{out}, can be computed by simply integrating the electric field over the readout and, given that the readout has $k+1$ elements, this implies:

$$U'_{out} = \sum_{i=m-k}^{m} \Phi'_i A'_i \Delta z'. \tag{23}$$

The preceding equations give, in a condensed and dimensionless form, a two-carrier electrostatic model of a quasi-one-dimensional SPRITE detector. In the next section, this model will be used to analyze the performance of given detectors, and also to synthesize new detector structures.

4. COMPUTATIONAL RESULTS

The model was implemented on a 486DX2/66-based desktop computer using a Microsoft FORTRAN compiler. We found that breaking the detector into $m = 100$ elements was sufficient to produce good results. This was confirmed by repeating the calculations with twice as many elements and observing no change in the output. We found that a complete analysis typically takes only 5 min of computation time.

The first task for the new model is the computation of the MTF of a simple non-tapered SPRITE detector. This is done both to test the model and also to observe any new phenomena not predicted by the previous work. Table 1 lists typical dimensionless ratios. These are computed from data drawn from Refs [5, 7]. These numbers will be used throughout the remainder of this paper.

Before responses can be produced, however, the detector must first be initialized to its steady state. The model is run without any inputs other than the constant background. The progress of the charge-equilibration process is monitored by observing the mean-square derivative. Figure 2 is a graph of the resulting electron and hole charge densities. Note the strong influence of the boundaries on the charge densities. This distribution is not simply exponential as predicted by the linear theories[8], however, because the electric field is no longer constant and the charge distribution is distorted.

To obtain the impulse response, a small charge input is scanned across the detector to mimic the process of scanning a small light spot. The input is taken to have a normalized width of $\Delta z'$, and it is moved $\Delta z'/n$ elements in $\Delta t'$ time. Figure 3 is a graph of such an impulse response. The pulse is approximately Gaussian, as predicted by the Green's function analysis. Two new features can be noted. First, the response is skewed to the right, because of causality and the boundary-blocking effect that delay charge transport and produce the slow exponential tail seen. Second, the response has a second small pulse that occurs just after the input spot begins to scan. This new pulse can be attributed to the voltage transient that must occur at the readout bias terminal that compensates for the new charge deposited near the other bias terminal. This peak is not important because of its small scale.

The voltage temporal response can be fast-Fourier tranformed to generate the frequency response of the

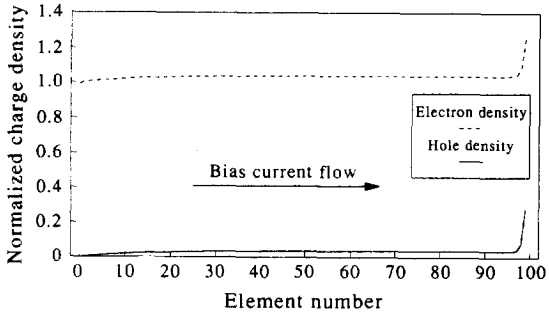

Fig. 2. Steady-state charge densities for constant background illumination. Notice the slow exponential rise near zero and the sharp apparent accumulation near 100.

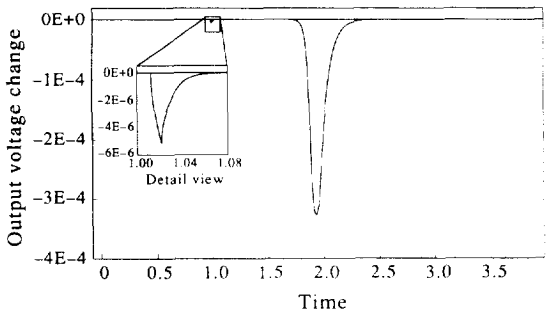

Fig. 3. Computed impulse response of typical detector. The main peak is skewed to the right, and there is a small secondary peak at the beginning of the scan (see inset).

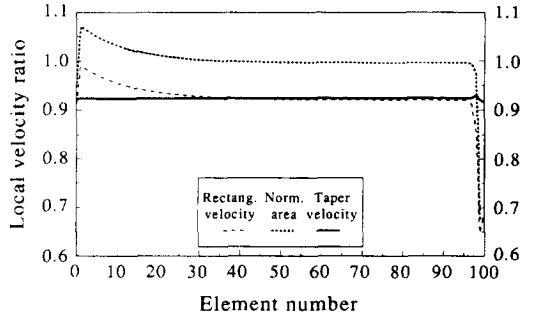

Fig. 5. The local ambipolar velocity ratio for the normal rectangular detector, and cross-sectional area and velocity ratio of the tapered detector.

detector. The normalized magnitude of this complex-valued function is the MTF. The graph of the MTF is shown in Fig. 4. Also shown for comparison is the MTF given by the Green's-function analysis[1]. The numerical analysis predicts a lower cut-off frequency than the classical analysis. This is caused by signal-degrading effects such as the boundary effects and the nonlinearity of transport.

As mentioned above, the actual drift velocity does not equal the nominal value and, further, it is not even a constant. The local ambipolar drift velocity at position i depends on several factors: the flux, the area, the concentration of electrons, and the concentration of holes. The ratio of this speed to the nominal speed is denoted α_i, and can be written:

$$\alpha_i = \frac{\Phi_i'}{A_i'} \times \frac{(n_i' + n_{i+1}' - p_i' - p_{i+1}')}{n_i' + n_{i+1}' + R_\mu(p_i' + p_{i+1}')}. \quad (24)$$

A graph of this velocity ratio is shown in Fig. 5. Considerable deviations are evident, especially at the boundaries. Without changing the parameters of the problem, the best scanning velocity available is given by the average value of the ambipolar velocity $\bar{\alpha}$. This average ratio is the correction constant used in eqn (19), and in this case has a value of about 0.92.

One approach cited in the literature to combat this speed variation is the variation of cross-sectional area along the device. With an appropriate variation or taper, the local velocity can be made almost constant. By using the following iterative rule relating the new area, $A'_{\text{new},i}$, to the previous area, $A'_{\text{old},i}$:

$$A'_{\text{new},i} = A'_{\text{old},i} \frac{\alpha_i}{\bar{\alpha}}, \quad (25)$$

the total mean-square deviation of the velocity can be reduced. By repeating the process of correction, the procedure will converge and produce a taper description. The taper obtained in this manner for the given parameters is also shown in Fig. 5.

The success of this taper pattern is demonstrated through the computation of the local velocity ratio, as shown in Fig. 5. Positive control of the velocity has been achieved, with a reduction of the mean-square deviation of over six orders of magnitude compared with the untapered detector. The MTF of the tapered detector, shown in Fig. 6, along with the MTF of the untapered SPRITE, shows some modest improvement. The increase is small because diffusive spreading of the charge is much more important than scan mismatch in our case, when the worst-case mismatch was only about 10%.

5. MODULATION-DOPED SPRITE

Tapering is used to obtain optimum performance within the basic SPRITE concept. Even the tapered

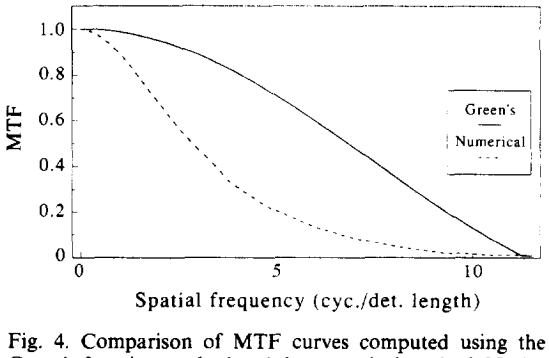

Fig. 4. Comparison of MTF curves computed using the Green's function method and the numerical method. Notice that the numerical solution is considerably lower than its analytical counterpart.

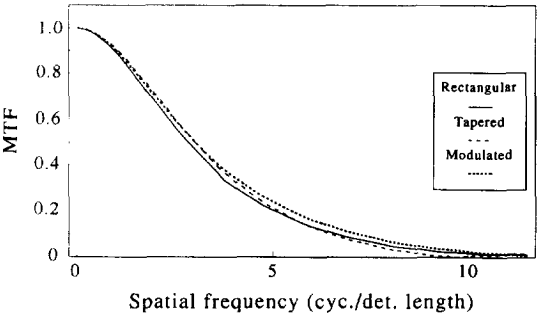

Fig. 6. The comparison of the MTF of the rectangular, tapered, and modulation-doped SPRITE detectors. The taper produces a better MTF at low and intermediate frequencies and a more definite zero in response about 10 cycles per detector length whereas the modulation-doped detector improves the response at all frequencies.

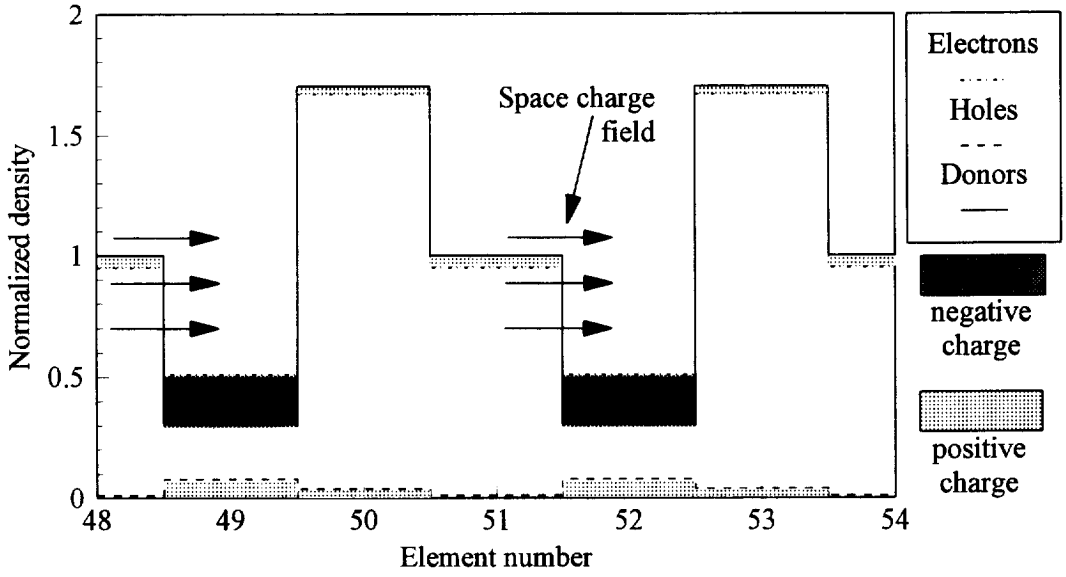

Fig. 7. The steady-state charge pattern of the modulation-doped SPRITE. The separation of positive and negative charge produces strong space-charge fields, which tend to prevent the backward motion of holes.

SPRITE suffers from the fundamental resolution limit of diffusion. One possible method to counteract the effect of diffusion is to build into the SPRITE some kind of structure that would curtail the spreading of charge. One method would be to modulate the doping level in each segment so that there would be a regular periodic structure along the length of the detector. Figure 7 shows the doping level for six segments near the middle of the detector. The doping is made to have a saw-tooth profile. This kind of doping variation has several impacts. The conductivity and thus the electric flux induced by the bias current varies from point to point. Second, the majority carriers will redistribute themselves under the influence of diffusion, which will cause the formation of space-charge fields. Third, the large variations in local carrier density will produce variations in the ambipolar mobility. Taken all together, it is suggested that this doping profile might reduce diffusion and improve the MTF.

The steady-state carrier distributions are also shown in Fig. 7 for the same six detector segments. The partial depletion of the highly-doped regions and the consequent over-charging of the lightly-doped regions can be seen, as indicated in Fig. 7 by the dark shading for negative charge and light shading for positive charge. This creates a permanent space-charge field in the structure; specifically, there is a high positive field interface in each cycle of the pattern, as shown. Any holes trying to travel backward across this boundary are impeded, which reduces the overall diffusion rate and improves performance. This can be seen by computing the MTF of the modulation-doped detector, shown in Fig. 6. Again, a small improvement in MTF can be seen. It should be noted that this result was achieved with a relatively simple doping profile. Revision and refinement of the profile might well provide further improvement.

6. CONCLUSIONS

In this work, a new model of carrier transport in SPRITE detectors is developed. This model uses a two-carrier electrostatic formalism to produce a system of discrete numerical equations that describe the motion of carriers in the detector. The model is one-dimensional in scale, but the provision for varying the detector cross-section enables the analysis of nonuniform photoconductor filaments. The steady-state carrier distributions produced show a marked deviation from those predicted by previous linear models. The impulse response derived is asymmetric and exhibits a second peak not explained by the classical theory. The MTF generated from this model predicts a lower spatial resolution than predicted by Green's function analysis and is in closer agreement with the measured data than previous analysis[9].

The model is then used to optimize the shape of a tapered detector. This technique is shown to improve uniformity of the ambipolar velocity and the MTF behavior of the final design. Further, the possibility of modulation-doping of the SPRITE is investigated. This doping reduces the diffusive spreading of carriers within the SPRITE. One possible doping profile is demonstrated to improve the MTF.

Acknowledgement—This work was supported by Westinghouse Electric Corporation, Orlando, Florida.

REFERENCES

1. G. D. Boreman and A. E. Plogstedt, *Appl. Opt.* **27,** 4331 (1988).
2. F. J. Effenberger and G. D. Boreman, *Appl. Opt.* **34,** 4651 (1995).
3. J. T. M. Wotherspoon, M. D. Johns, T. Ashley, C. T. Elliott and A. M. White, *IEE Conf.* **228,** 67 (1983).
4. T. Ashley, C. T. Elliot, A. M. White, J. T. M. Wotherspoon and M. D. Johns, *Infrared Phys.* **24,** 25 (1994).
5. A. Campbell, C. T. Elliott and A. M. White, *IEE Conf.* **263,** 18 (1986).
6. A. Campbell, C. T. Elliott and A. M. White, *Infrared Phys.* **27,** 125 (1987).
7. A. P. Davis, *Infrared Phys.* **33,** 301 (1992).
8. T. Ashley and C. T. Elliott, *Infrared Phys.* **22,** 367 (1982).
9. K. J. Barnard, G. D. Boreman, A. E. Plogstedt and B. K. Anderson, *Appl. Opt.* **31,** 144 (1992).